AIAA 2005-5921

Aerodynamic Parameter Estimation for the X-43A (Hyper-X) from Flight Data

Eugene A. Morelli

Stephen D. Derry

NASA Langley Research Center
Hampton, VA

Mark S. Smith

NASA Dryden Flight Research Center
Edwards, CA

AIAA Atmospheric Flight Mechanics Conference and Exhibit
August 15-18, 2005 / San Francisco, CA

Aerodynamic Parameter Estimation for the X-43A (Hyper-X) from Flight Data

Eugene A. Morelli* and Stephen D. Derry†
NASA Langley Research Center, Hampton, Virginia, 23681-2199, USA

Mark S. Smith‡
NASA Dryden Flight Research Center, Edwards, California, 93523-0273, USA

Aerodynamic parameters were estimated based on flight data from the third flight of the X-43A hypersonic research vehicle, also called Hyper-X. Maneuvers were flown using multiple orthogonal phase-optimized sweep inputs applied as simultaneous control surface perturbations at Mach 8, 7, 6, 5, 4, and 3 during the vehicle descent. Aerodynamic parameters, consisting of non-dimensional longitudinal and lateral stability and control derivatives, were estimated from flight data at each Mach number. Multi-step inputs at nearly the same flight conditions were also flown to assess the prediction capability of the identified models. Prediction errors were found to be comparable in magnitude to the modeling errors, which indicates accurate modeling. Aerodynamic parameter estimates were plotted as a function of Mach number, and compared with estimates from the pre-flight aerodynamic database, which was based on wind-tunnel tests and computational fluid dynamics. Agreement between flight estimates and values computed from the aerodynamic database was excellent overall.

Nomenclature

a_x, a_y, a_z	body-axis translational accelerometer measurements, ft/sec^2
Cov	covariance matrix
$E\{\ \}$	expectation operator
J	cost function
M	Mach number
max	maximum
min	minimum
p,q,r	body-axis roll, pitch, and yaw rates, rad/sec
$\bar{q}$	dynamic pressure, lbf/ft^2
rms	root-mean-square
s	standard error
V	airspeed, ft/sec
x_{cg}, y_{cg}, z_{cg}	coordinates of the center of gravity
x_{cg}, y_{cg}, z_{cg}	coordinates of the reference point
α	angle of attack, deg
β	sideslip angle, deg

* Research Engineer, Dynamic Systems and Control Branch, MS 308, Associate Fellow
† Research Engineer, Dynamic Systems and Control Branch, MS 308
‡ Research Engineer, Aerodynamics Branch, P.O. Box 273

$\delta_e, \delta_a, \delta_r$	symmetric elevon, asymmetric elevon, and rudder deflections, deg
$\boldsymbol{\theta}$	parameter vector
σ^2	variance

superscripts

T	transpose
$\hat{}$	estimate
$\tilde{}$	Fourier transform
–1	matrix inverse
$\dagger$	complex conjugate transpose

I. Introduction

On November 16, 2004, flight 3 of the NASA X-43A hypersonic research vehicle, or Hyper-X, was successfully conducted over the Pacific Ocean off the California coast. Figures 1 and 2 show the X-43A research vehicle. The flight included a successful test of the scramjet propulsion system at approximately Mach 10. Following the engine test, the engine cowl door was closed, and a series of maneuvers were executed for aerodynamic parameter estimation as the vehicle descended and Mach number decreased. Maneuvers were executed for flight conditions at Mach 8, 7, 6, 5, 4, and 3. The vehicle flew as a glider (engine off) throughout these maneuvers.

Figure 1 X-43A research vehicle

The descent maneuvers were executed using multiple orthogonal phase-optimized sweep inputs[1] on all three control surface inputs - symmetric elevon, asymmetric elevon, and rudder. Since flight conditions change rapidly during the descent, the inputs were designed to be applied simultaneously, so that a full set of non-dimensional longitudinal and lateral stability and control derivatives could be estimated at each flight condition. The flight testing also included multi-step 2-1-1 waveforms applied to each of the control surface inputs in sequence, following the sweep inputs. Flight data from the 2-1-1 maneuvers were used to test the prediction capability of the models identified from the sweep inputs. Accurate prediction for maneuvers with dissimilar inputs is a strong indicator of good modeling results.

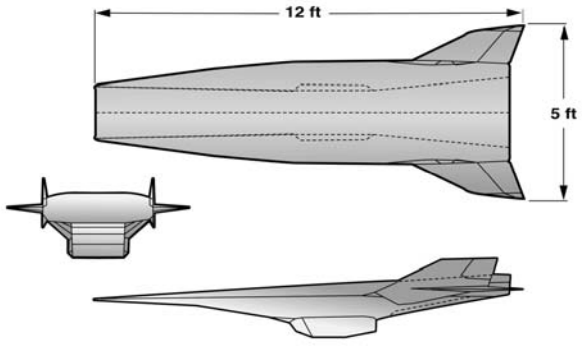

Figure 2 X-43A research vehicle 3-view

Aerodynamic parameters estimated from flight data for the Hyper-X are useful for comparisons with results from wind tunnel tests and computational fluid dynamics (CFD), to validate and refine aerodynamic prediction methods for designing future hypersonic vehicles. Flight-determined aerodynamic parameters can also be used to update the aerodynamic database for Hyper-X, for improved simulation and dynamic analysis.

The purpose of this paper is to explain and document the experiment design, data analysis, and modeling results for the parameter estimation maneuvers flown as part of flight 3 of the X-43A hypersonic research vehicle. Flight 2 results were reported previously[2], and flight 1 was aborted because of a roll instability and subsequent structural failures on the booster during the launch phase[3].

The next section describes how the multiple orthogonal phase-optimized sweep inputs were designed and the methods used for aerodynamic modeling based on flight data. Following this, a short description is given of the

X-43A hypersonic research vehicle and the flight data. Finally, aerodynamic modeling results are presented, including accuracy of the estimated parameters, and comparisons with the pre-flight aerodynamic database. Prediction capability of the models identified from the sweep data is demonstrated using flight data from a multi-step 2-1-1 maneuver.

II. Methods

A. Input Design

The method used to design the inputs for the parameter estimation maneuvers is described in Ref. 1. The general idea is to excite the vehicle with wide-band inputs containing frequencies in the range where the modal frequencies of the vehicle dynamic response are expected, using an input form that is efficient for parameter estimation. Each input is comprised of a sum of sinusoids with unique frequencies. The following material describes in detail how the multiple orthogonal phase-optimized sweeps were designed and why this particular input form is efficient for parameter estimation. The wide-band nature of the inputs is important because there is naturally some uncertainty as to the exact modal frequencies for the vehicle in flight. Wide-band inputs provide robustness to this uncertainty.

The time length T allotted for each maneuver was fixed at 30 seconds for practical reasons. Harmonic sinusoids with unique frequencies, tightly spaced within the assumed frequency range, comprised the pool of spectral components from which specific components were selected to create each designed input. Each input had the form

$$\boldsymbol{u} = \sum_{k \in \{1,2,..,M\}} A_k \cos\left(\frac{2\pi k \boldsymbol{t}}{T} + \phi_k\right) \tag{1}$$

where A_k and ϕ_k were the amplitude and phase for the k^{th} sinusoidal component, and each input was comprised of selected components from the pool of M sinusoids with frequencies $\omega = 2\pi k/T$, $k = 1,2,\ldots,M$.

The sinusoidal components, each with a unique frequency, were allocated to the three effective control surface inputs for the X-43A – symmetric elevon, asymmetric elevon, and rudder. Allocated frequencies were interleaved to achieve a wide frequency spectrum for each input, as shown in Figure 3. This provided robustness to uncertainty in detailed knowledge of how each control would excite the dynamic modes of the vehicle. Furthermore, there was a practical limit on flight computer memory available to implement the perturbation inputs for aerodynamic parameter estimation. Consequently, a single set of excitation inputs had to be applied at all flight conditions throughout the descent. The wide-band frequency content and uniform power distribution of the inputs made it possible to satisfy this practical constraint without compromising the effectiveness of the excitation.

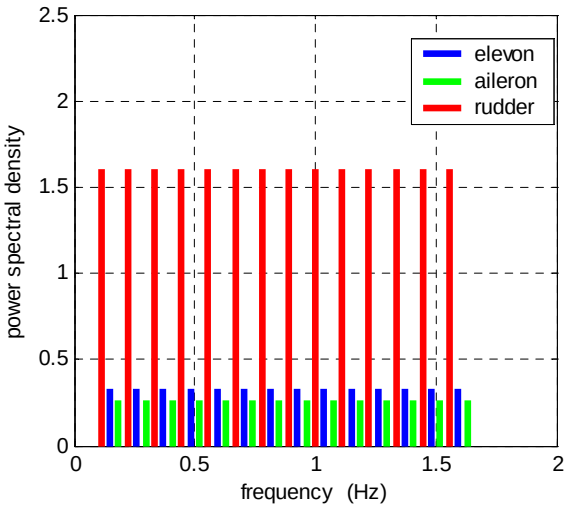

Figure 3 Multiple orthogonal phase-optimized sweep input spectra, Mach 6

For each input individually, an optimization routine adjusted the phases of the sinusoidal components to minimize the relative peak factor, with the constraint that the input must start and end at zero, since each input must be a perturbation from a reference condition.

Relative peak factor is a measure of the efficiency of an input for parameter estimation purposes, in terms of the amplitude range of the input divided by a measure of the input energy. The relative peak factor *RPF* for an input $\boldsymbol{u}$ is defined by

$$RPF(\boldsymbol{u}) = \frac{\left[max(\boldsymbol{u}) - min(\boldsymbol{u}) \right]}{2\sqrt{2}\ rms(\boldsymbol{u})} \tag{2}$$

For a single sinusoidal component, *RPF*=1. For a composite signal with more than one sinusoidal component, as in Eq. (1), the goal is to design the input for minimum *RPF*. This is done by adjusting the phase parameters ϕ_k for the components of each input to minimize *RPF*. The resulting optimization problem is non-convex; however, a simplex algorithm can be applied to find a solution, see Ref. 1.

Inputs with low relative peak factors are desirable for parameter estimation, where the objective is to excite the system as much as possible (quantified by the input energy measure $rms(\boldsymbol{u})$), without causing responses to deviate far from the reference condition (quantified by the input amplitude range measure $\left[max(\boldsymbol{u}) - min(\boldsymbol{u}) \right]$).

For each input, power was distributed uniformly over the spectral components, which means that

$$A_k = \frac{A}{\sqrt{n}} \quad \forall\, k \tag{3}$$

where n is the number of sinusoidal components included in the summation of Eq. (1), and A is the amplitude of the composite input $\boldsymbol{u}$. Therefore, with uniform power distribution, selection of the A_k reduces to selecting a single input amplitude A.

Amplitudes for the three inputs were selected based on test runs of a nonlinear simulation of the Hyper-X, which used aerodynamic data from wind tunnel tests and CFD, and included the feedback control system. The aim was to scale the inputs to achieve response amplitudes of approximately ±3 deg in angle of attack and sideslip angle perturbations for each maneuver, based on the simulation. Input amplitude adjustments were done by trial-and-error, because the feedback control system distorted the perturbation inputs for parameter estimation in a manner that depended on the vehicle response.

All of the inputs designed in this way were mutually orthogonal in both the time and frequency domains. The orthogonality is the result of assigning unique frequencies to each input (frequency-domain orthogonality, cf. Figure 3) and using sinusoids with frequencies that are multiples of a common fundamental frequency (time-domain orthogonality). Figure 4 shows the multiple orthogonal phase-optimized sweep perturbation inputs that were applied at Mach 6. The same input forms were used at every flight condition from Mach 8 to Mach 3, but the amplitudes of the inputs were adjusted to account for the changing dynamic pressure and control surface effectiveness. This approach was taken because of a practical limitation on flight computer memory, as mentioned above.

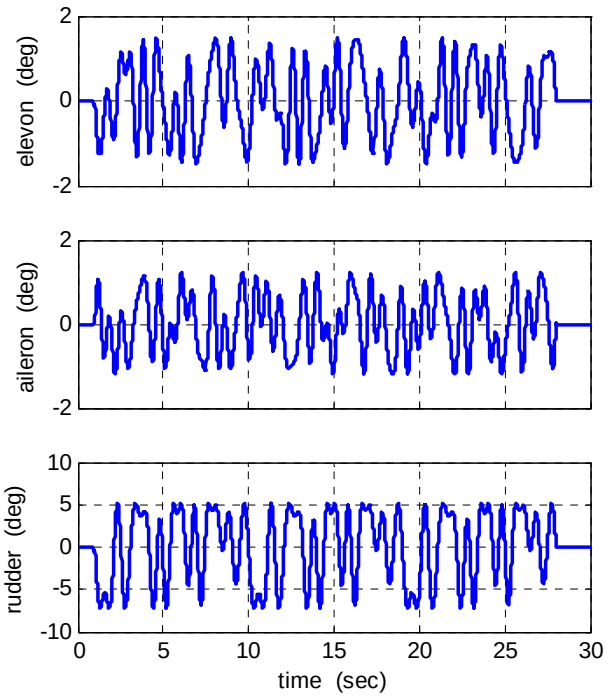

Figure 4 Multiple orthogonal phase-optimized sweep inputs, Mach 6

Orthogonal inputs are advantageous for parameter estimation experiments, because the aerodynamic dependencies can be assigned more accurately when all inputs are doing something different to excite the dynamic response of the vehicle. The orthogonality of the designed inputs was disrupted during the flight testing of the X-43A, due to the action of the feedback control, which could not be turned off. However, starting out with

orthogonal inputs prevented the feedback control from correlating the inputs to the point where the modeling results would be adversely impacted.

The multi-step 2-1-1 maneuvers used for prediction tests were designed very simply by using the characteristic waveform of a 2-1-1 multi-step, which is three adjacent square-wave pulses with alternating sign and pulse widths in the ratio 2-1-1. The width of the "1" pulse was selected as 1 second, so that the frequency content of the input would be close to the natural frequency of the expected dominant dynamic response. This approach produced an input designed to excite the dynamic response using a waveform very different from the sweeps used for the modeling, described earlier. Consequently, the 2-1-1 multi-step provided a good test of model prediction capability.

B. Model Structure Determination

Stepwise regression[4] and orthogonal function modeling[5] were used to determine the model structure for parameter estimation. These methods are included in a software toolbox written in MATLAB®[6], called System IDentification Programs for AirCraft (*SIDPAC*)[7], developed at NASA Langley. The methods use orthogonalization and statistical metrics to select terms for an adequate model, based on the measured data. Each method was applied separately, to cross-check the identified model structure.

In all cases, a linear aerodynamic model was found to be adequate to characterize the measured data. The aerodynamic model equations were

$$C_L = C_{L_\alpha}\alpha + C_{L_{\delta_e}}\delta_e + C_{L_o} \tag{4}$$

$$C_D = C_{D_\alpha}\alpha + C_{D_{\delta_e}}\delta_e + C_{D_o} \tag{5}$$

$$C_m = C_{m_\alpha}\alpha + C_{m_q}\frac{q\bar{c}}{2V} + C_{m_{\delta_e}}\delta_e + C_{m_o} \tag{6}$$

$$C_Y = C_{Y_\beta}\beta + C_{Y_{\delta_r}}\delta_r + C_{Y_o} \tag{7}$$

$$C_l = C_{l_\beta}\beta + C_{l_{\delta_a}}\delta_a + C_{l_{\delta_r}}\delta_r + C_{l_o} \tag{8}$$

$$C_n = C_{n_\beta}\beta + C_{n_{\delta_a}}\delta_a + C_{n_{\delta_r}}\delta_r + C_{n_o} \tag{9}$$

where all state and control variables are perturbations from a reference condition, defined at the beginning of each maneuver.

Lift and drag coefficients were used instead of the body-axis *x* and *z* components of aerodynamic force, so that the flight results could be compared directly to values from the pre-flight aerodynamic database, which was based on extensive wind tunnel data with CFD augmentation. Aerodynamic moment coefficients were modeled at the aerodynamic reference point used for the aerodynamic database, again to facilitate comparisons.

For all flight conditions studied, the pitch rate damping was the only rate derivative term that had a significant effect on the X-43A aerodynamics. Model terms associated with other rate derivatives were dropped during model structure determination, because the models given in the above equations almost completely characterized the variations in the associated force or moment coefficient. This simply means that rate damping terms were not necessary to model the lift, drag, side force, or lateral moment coefficients, so the damping terms were omitted from those models. Equivalently, the damping parameters were zero for these force and moment coefficients, based on the data.

C. Parameter Estimation

The aerodynamic model parameters in Eqs. (4)-(9) can be estimated from flight data using linear regression or output-error maximum likelihood in the time-domain or frequency-domain, among other approaches[8]. Software that implements each of these methods is included in *SIDPAC*, and these tools were applied to the data from flight 3. However, the most consistent results, and those that exhibited the best prediction capability, came from equation-error in the frequency domain. This was also true for the flight 2 data analysis and modeling[2]. Consequently, all of the parameter estimation results shown in this work were computed using equation-error in the frequency domain. A brief outline of that method is given below. Additional information on this approach can be found in Refs. 8 and 9.

The equation-error method calculates aerodynamic parameter estimates that minimize squared errors between values of the non-dimensional force and moment coefficients determined from measured flight data, and model values computed from Eqs. (4)-(9). For a glider, non-dimensional force and moment coefficients are determined from measured flight data using the following equations:

$$C_X \equiv -C_A = \frac{m a_x}{\bar{q} S} \tag{10}$$

$$C_Y = \frac{m a_y}{\bar{q} S} \tag{11}$$

$$C_Z = -C_N = \frac{m a_z}{\bar{q} S} \tag{12}$$

$$C_L = -C_Z \cos\alpha + C_X \sin\alpha \tag{13}$$

$$C_D = -C_X \cos\alpha - C_Z \sin\alpha \tag{14}$$

$$C_l = \frac{I_x}{\bar{q} S b}\left[\dot{p} - \frac{I_{xz}}{I_x}\left(pq + \dot{r} \right) + \frac{\left(I_z - I_y \right)}{I_x} qr \right] \tag{15}$$

$$C_m = \frac{I_y}{\bar{q} S \bar{c}}\left[\dot{q} + \frac{\left(I_x - I_z \right)}{I_y} pr + \frac{I_{xz}}{I_y}\left(p^2 - r^2 \right) \right] \tag{16}$$

$$C_n = \frac{I_z}{\bar{q} S b}\left[\dot{r} - \frac{I_{xz}}{I_z}\left(\dot{p} - qr \right) + \frac{\left(I_y - I_x \right)}{I_z} pq \right] \tag{17}$$

Substituting measured data into the right sides of Eqs. (10)-(17) results in N values of the non-dimensional force and moment coefficients, where N is the number of data points for the maneuver. Using these values and measured states and controls in Eqs. (4)-(9) results in an over-determined set of equations for the unknown aerodynamic parameters, which can be solved with a standard least-squares method.

For example, the least-squares problem for the lift coefficient was formulated using the model structure in Eq. (4) as

$$\boldsymbol{z} = \boldsymbol{X\theta} + \boldsymbol{\nu} \tag{18}$$

where

$\boldsymbol{z} = \left[C_L(1) \;\; C_L(2) \;\; \ldots \;\; C_L(N) \right]^T = N \times 1$ vector of values computed from Eqs. (10), (12), and (13)

$\boldsymbol{\theta} = \left[C_{L_o} \;\; C_{L_\alpha} \;\; C_{L_{\delta_e}} \right]^T = 3 \times 1$ vector of unknown parameters

$\boldsymbol{X} = \left[\mathbf{1} \;\; \boldsymbol{\alpha} \;\; \boldsymbol{\delta_e} \right] = N \times 3$ matrix of vectors of ones and explanatory variables

$\boldsymbol{\nu} = \left[\nu(1) \;\; \nu(2) \;\; \ldots \;\; \nu(N) \right]^T = N \times 1$ vector of equation errors

The best estimator of $\boldsymbol{\theta}$ in a least-squares sense comes from minimizing the sum of squared differences between the measurements and the model,

$$J(\boldsymbol{\theta}) = \frac{1}{2} (\boldsymbol{z} - \boldsymbol{X\theta})^T (\boldsymbol{z} - \boldsymbol{X\theta}) \tag{19}$$

The least-squares solution for the unknown parameter vector $\boldsymbol{\theta}$ is[8]

$$\hat{\boldsymbol{\theta}} = \left(\boldsymbol{X}^T \boldsymbol{X} \right)^{-1} \boldsymbol{X}^T \boldsymbol{z} \tag{20}$$

The estimated parameter covariance matrix is computed from[8]

$$Cov\left(\hat{\boldsymbol{\theta}}\right) = E\left[\left(\hat{\boldsymbol{\theta}} - \boldsymbol{\theta}\right)\left(\hat{\boldsymbol{\theta}} - \boldsymbol{\theta}\right)^T \right] = \hat{\sigma}^2 \left(\boldsymbol{X}^T \boldsymbol{X} \right)^{-1} \tag{21}$$

$$\hat{\sigma}^2 = \frac{(\boldsymbol{z} - \hat{\boldsymbol{y}})^T (\boldsymbol{z} - \hat{\boldsymbol{y}})}{\left(N - n_p \right)} \qquad ; \qquad \hat{\boldsymbol{y}} = \boldsymbol{X}\hat{\boldsymbol{\theta}} \tag{22}$$

where the number of unknown parameters $n_p = 3$ for this example.

To apply equation-error parameter estimation in the frequency domain, the data is first transformed from the time domain into the frequency domain. For parameter estimation purposes, this can be done very effectively using a high-accuracy chirp-*z* Fourier transform, with the capability to use arbitrary frequencies for the transformation[10]. The resulting set of over-determined equations is of the same form given in Eq. (18) above, except that the number of data points is now *m*, corresponding to the number of selected frequencies for the Fourier transformation, and the problem now involves complex numbers. The analogs of Eqs. (20)-(22) for equation-error in the frequency domain are[8]

$$\hat{\boldsymbol{\theta}} = \left[Re\left(\tilde{\boldsymbol{X}}^\dagger \tilde{\boldsymbol{X}} \right) \right]^{-1} Re\left(\tilde{\boldsymbol{X}}^\dagger \tilde{\boldsymbol{z}} \right) \tag{23}$$

$$Cov\left(\hat{\boldsymbol{\theta}}\right) = \hat{\sigma}^2 \left[Re\left(\tilde{\boldsymbol{X}}^\dagger \tilde{\boldsymbol{X}} \right) \right]^{-1} \equiv \left[C_{ij} \right] \quad i, j = 1,2,\ldots,n_p \tag{24}$$

$$\hat{\sigma}^2 = \frac{\left(\tilde{\boldsymbol{z}} - \hat{\tilde{\boldsymbol{y}}} \right)^\dagger \left(\tilde{\boldsymbol{z}} - \hat{\tilde{\boldsymbol{y}}} \right)}{m - n_p} \quad ; \quad \hat{\tilde{\boldsymbol{y}}} = \tilde{\boldsymbol{X}}\hat{\boldsymbol{\theta}} \tag{25}$$

Eqs. (23)-(25) were used to compute equation-error parameter estimates and the associated covariance matrix. The standard errors of the estimated parameters are given by the square roots of the diagonal elements of the covariance matrix,

$$s\left(\hat{\theta}_j\right) = \sqrt{Var\left(\hat{\theta}_j\right)} = \sqrt{C_{jj}} \quad j = 1,2,\ldots,n_p \tag{26}$$

Since the parameter estimation was done in the frequency domain, there was no need to correct the estimated parameter standard errors for colored residuals, see Ref. 8.

III. Research Vehicle and Experimental Data

Figure 1 shows an artist's rendering of the X-43A research vehicle in flight. A 3-view drawing is shown in Figure 2. At the start of the mission, the X-43A research vehicle was mounted to the nose of a modified Pegasus booster. This configuration, called the Hyper-X stack, was carried to 40,000 ft by the NASA B-52B aircraft in a manner similar to the X-1 flight tests. Figure 5 is a picture of the Hyper-X stack being carried to altitude for flight 3. At the target flight condition, the Hyper-X stack was dropped, and the Pegasus booster fired about 5 seconds later. The Pegasus booster carried the X-43A to the target flight condition for the scramjet engine test, which was approximately Mach 10 and 100,000 ft altitude. At that point, the X-43A separated from the Pegasus booster, and began its free flight. After stabilization at the target flight condition, the engine cowl was opened and the scramjet engine test was conducted. Then, the engine cowl door closed, and the X-43A executed an energy reduction maneuver to arrive at the Mach 8 flight condition. Perturbation inputs for aerodynamic parameter estimation, control law validation, and aerodynamic prediction were then run automatically, and these were repeated at Mach 7, 6, 5, 4, 3, and 2 during the vehicle descent. The vehicle then splashed into the Pacific ocean and was not recovered. Figure 6 shows a graphical depiction of the X-43A mission profile. Note that the data at Mach 2 was not usable for parameter estimation, because at that flight condition, the vehicle encountered wind shears and gusts which were unmeasured and therefore corrupted the parameter estimation results. Consequently, flight 3 results did not include the Mach 2 flight condition.

Figure 5 Hyper-X stack being carried to altitude on the NASA B-52B

Ref. 11 includes complete information on the geometry and mass properties of the X-43A research vehicle. Table 1 gives a summary of the constant mass and geometry values used for the analysis. The mass properties reflect the fully loaded X-43A research vehicle minus the mass of fuel and coolant used during the scramjet engine test.

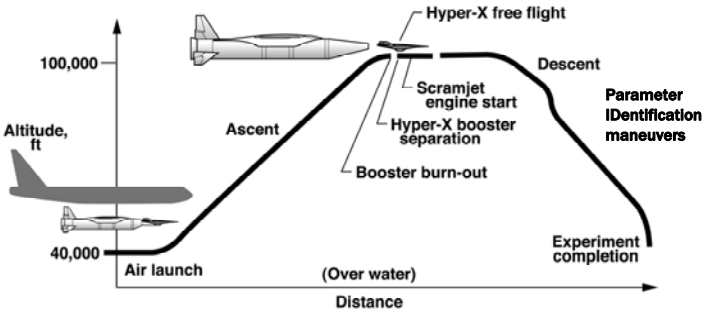

Figure 6 Hyper-X mission profile

Flight data came from the Best Estimated Trajectory (BET), documented in Refs. 11 and 12. The BET data set used the best data from several recorded sources, corrected for known time skews and estimated winds aloft. The BET data were also corrected for systematic instrumentation errors using a data compatibility analysis. Sample rate for the BET flight data was 50 Hz, corresponding to a sampling interval of 0.02 sec.

All parameter estimation was done for the aerodynamic forces and moments acting at the model reference point, which is the reference point for the aerodynamic database. This was done to facilitate comparisons between stability and control derivatives from the aerodynamic database and estimates based on flight data. The same approach was used for the flight 2 results documented in Ref. 2. Details of the location of the model reference point are available in Ref. 11. Coordinates of the reference point are [66.24, 0.00, 0.00] inches in a standard right-handed coordinate frame using fuselage station, butt line, and water

line coordinates, as defined in Ref. 11. The aerodynamic reference point is about 5.5 feet aft of the nose, on the vehicle centerline.

IV. Results

Aerodynamic parameters were estimated from flight data using equation-error in the frequency domain and linear model structures, as explained in section II. The transformation of time domain data into the frequency domain was done using the frequencies [2/*T*, 2/*T* +0.005, 2/*T* + 0.010, …, 2.0] Hz, where *T* was the time length of the maneuver in seconds. This selection of frequencies included at least two cycles for each frequency over the length of the maneuver *T*, with a very fine frequency resolution to capture details in the frequency domain. The 2 Hz upper limit for the frequency band was selected so that all deterministic frequency content was included, but wide-band noise was automatically filtered by the transformation. This approach enhances signal-to-noise ratio, and improves modeling results, while retaining all useful information for parameter estimation in the frequency domain. Conversion to the frequency domain was done using the high-accuracy Fourier transform from Ref. 10, which allows selection of the transformation frequencies, independent of the length of the maneuver *T*. The accuracy of this transformation is on the order of the round-off error of the computer.

Estimates for stability and control derivatives associated with the lift coefficient are plotted in Figure 7 as a function of Mach number. The triangles represent flight estimates computed from Eq. (23), and the circles are values computed from table look-ups in the pre-flight aerodynamic database. The aerodynamic database was built from data collected during extensive wind tunnel testing, with some CFD augmentation, see Ref. 13. Error bars on all estimates indicate ±2 standard errors, corresponding to 95% confidence, assuming a Gaussian distribution. Error bars for the aerodynamic database values represent an estimated uncertainty, computed based on the uncertainty model documented in Ref. 14. Error bars for the flight estimates came from Eqs. (24)-(26).

Numbers on vertical axes for the parameter estimate plots have been removed, because the numerical results are restricted to U.S. government employees and U.S. government contractors only. However, the scales have not been altered, so the relative positions of the estimates and sizes of the error bars are real. Complete numerical results are available in Ref. 15, which is a restricted document.

Similar plots for drag coefficient parameters and pitching moment coefficient parameters are shown in Figures 8 and 9, using the same presentation format. Side force, rolling moment, and yawing moment coefficient parameters appear in Figures 10, 11, and 12, respectively. Inspection of these plots shows that the flight estimates were generally in excellent agreement with values obtained from the pre-flight aerodynamic database. This is indicated by flight estimates usually lying within the uncertainty bounds of the corresponding value from the aerodynamic database. In addition, the flight estimates had small error bars, indicating accurate parameter estimates. The standard errors for the flight estimates were less than 5 percent of the estimated values, for all parameters except the pitch rate derivative.

As discussed earlier, the pitch rate damping was the only rate derivative term that had a significant effect on the X-43A aerodynamics. Consequently, there are no plots in Figures 7, 8, 10, 11, or 12 associated with damping derivatives.

The pitch damping in Figure 9 shows what looks like a significant mismatch between flight estimates and the aerodynamic database. However, the C_{m_q} parameter multiplies the quantity $q\bar{c}/2V$ in the model equations, cf. Eq. 6. At Mach 5, for example, the value of $q\bar{c}/2V$ is 0.0006 for $q = 0.5$ rad/sec, which means that the value of C_{m_q} must be quite large in order for the damping term $C_{m_q}\dfrac{q\bar{c}}{2V}$ to be a non-trivial contributor in the model of Eq. (6). In fact, the estimates of C_{m_q} shown in Figure 9 were small in magnitude, so that the mismatch seen for the C_{m_q} estimates makes very little difference in the pitching moment computed from Eq. (6). The possibility of a numerical problem in the parameter estimation arising from the relatively small value of $q\bar{c}/2V$ compared to the other explanatory variables in the model was examined and ruled out.

Modeling results from flights 2 and 3 could not be compared for maneuvers executed at similar Mach numbers, because the flight conditions were different. Consequently, it was more meaningful to compare flight 3 estimates to

values extracted from the aerodynamic database at the same flight conditions, rather than to compare flight estimates at similar Mach numbers for flights 2 and 3. The maneuvers at similar Mach numbers on flights 2 and 3 had dissimilar values of important flight condition parameters such as nominal angle of attack and elevator deflection. Agreement of flight 2 parameter estimation results with values from the aerodynamic database (cf. Refs. 2 and 15) was very similar to that seen in Figures 7 through 12 for flight 3.

Figure 13 shows a typical model fit to the flight data. This particular example is the model fit to the pitching moment coefficient at Mach 5 on flight 3. The excellent fit quality is typical of the other cases as well. The upper plot in Figure 13 shows the model fit to the data in the frequency domain, the middle plot shows the model fit to the data in the time domain, and the lower plot shows the difference between the two traces in the middle plot, which is the residual in the time domain, $z - \hat{y}$. The residual shows no deterministic content, indicating that the model has captured all of the deterministic variation. Note that the time-domain model includes a time-domain least-squares estimate of bias and linear trend with time in the measured output, because these terms are omitted when modeling in the frequency domain.

In Figure 14, the model identified using the sweep data shown in Figure 13 was used to predict the pitching moment coefficient at a similar Mach number (approximately Mach 5), using a different input, namely a 2-1-1 multi-step. The upper plot shows the 2-1-1 command to the symmetric elevon and the measured symmetric elevon position. The commanded symmetric elevon was modified by feedback control. The middle plot shows the time-domain prediction of pitching moment coefficient and the lower plot is the residual, or the difference between the two traces in the middle plot. The quality of the model fit to the prediction data is similar to that seen in Figure 13, indicating that the identified model is a good predictor for a dissimilar maneuver at similar flight conditions. Good prediction capability is a very strong indicator of an accurate model. The quality of the prediction result shown in Figure 14 was typical of the prediction results for the other models and flight conditions.

Slight mismatches toward the end of the prediction maneuver in Figure 14 might be attributable to changes in the vehicle aerodynamics due to rapidly changing Mach number during the descent. Figure 15 shows the Mach number variation over the time corresponding to the sweep input (done first), followed by a control system validation sweep at higher frequency, then finally the 2-1-1 prediction maneuver. The Mach number change over this period of time is approximately –0.75, so the model identified from data near the start of the time period may be slightly inapplicable for the prediction maneuver executed near the end of the time period.

V. Conclusions

The hypersonic aerodynamics of the X-43A were modeled with very high accuracy using linear model structures. Accurate models for all non-dimensional aerodynamic force and moment coefficients were identified from flight data at Mach 8, 7, 6, 5, 4, and 3, using equation-error parameter estimation in the frequency domain. Multiple orthogonal phase-optimized sweep inputs were shown to be good practical inputs for aerodynamic modeling. These wide-band inputs provided sufficient excitation to the vehicle in spite of a feedback control system that distorted the desired input forms. The resulting flight data had sufficient information content for the extraction of highly accurate estimates of aerodynamic stability and control derivatives. Standard errors for the aerodynamic parameters estimated from flight data were less than 5 percent for all parameters except the pitch damping derivative. Predictions using flight data from multi-step 2-1-1 maneuvers at similar flight conditions showed that the models identified using data from the multiple orthogonal phase-optimized sweeps had good prediction capability for maneuvers with dissimilar input forms. All of these results support high confidence in the models identified from flight data.

For all flight conditions studied, the rate damping terms were very small or zero in all axes, indicating that the vehicle aerodynamics were largely insensitive to non-dimensional angular rates. The X-43A was found to be statically stable in all axes with no control reversals. Overall, stability and control derivatives computed from the pre-flight aerodynamic database were found to be remarkably consistent with the flight estimates.

VI. References

[1]Morelli, E.A. "Multiple Input Design for Real-Time Parameter Estimation in the Frequency Domain," Paper REG-360, *13th IFAC Symposium on System Identification*, Rotterdam, The Netherlands, August 2003.

[2]Morelli, E.A., Derry, S.D., and Smith, M.S. "Aerodynamic Parameter Estimation for Flight 2 of the X-43A," Paper No. 20, *Joint Army Navy NASA Air Force (JANNAF) Conference*, Charleston, SC, June 2005 (classified).

[3]Dornheim, M.A. "X-43A To Fly in Fall", *Aviation Week and Space Technology*, 28 July 2003, pp. 36-37.

[4]Klein, V., Batterson, J.G., and Murphy, P.C. "Determination of Airplane Model Structure from Flight Data by Using Modified Stepwise Regression," NASA TP-1916, 1981.

[5]Morelli, E.A. and DeLoach, R., "Wind Tunnel Database Development using Modern Experiment Design and Multivariate Orthogonal Functions," AIAA Paper 2003-0653, *41st AIAA Aerospace Sciences Meeting and Exhibit*, Reno, NV, January 2003.

[6]*Using MATLAB® Version 6*, The MathWorks, Inc., Natick, MA, 2000.

[7]Morelli, E.A. (2002) "System IDentification Programs for AirCraft (*SIDPAC*)," AIAA Paper 2002-4704, *AIAA Atmospheric Flight Mechanics Conference*, Monterey, CA, August 2002.

[8]Klein, V. and Morelli, E.A. *Aircraft System Identification – Theory and Practice*, AIAA Education Series, AIAA, Reston, VA, to be published in 2006.

[9]Klein, V. "Aircraft Parameter Estimation in Frequency Domain," AIAA Paper 78-1344, *AIAA Atmospheric Flight Mechanics Conference*, Palo Alto, CA, August 1978.

[10]Morelli, E.A. "High Accuracy Evaluation of the Finite Fourier Transform using Sampled Data," NASA TM 110340, 1997.

[11]Del Corso, J.A. "X-43A Flight 3 Data Release," HX-1077, May 2005.

[12]Karlgaard, C. and Tartabini, P.V. "Best Estimated Trajectory Reconstruction for the X-43A Mach 7 and 10 Flights," Paper No. 17, *Joint Army Navy NASA Air Force (JANNAF) Conference*, Charleston, SC, June 2005.

[13]Engelund, W. C., Holland, S. D., Cockrell, C., E., Bittner, R. D. "Aerodynamic Database Development for the Hyper-X Airframe Integrated Scramjet Propulsion Experiment," *Journal of Spacecraft and Rockets*, Vol. 38, No. 6, pp. 803-810, Nov-Dec, 2001.

[14]White, J.T. "HXRV First-Flight Aerodynamic Uncertainty Model," DFRC-HX-0082, November 1999.

[15]Morelli, E.A. "Aerodynamic Modeling for the X-43A (Hyper-X) from Flight Data," NASA TM, to be published in 2005.

Table 1 Geometry and mass properties of the X-43A research vehicle for flight 3 descent

length $\bar{c}$, ft	12.00
wing span b, ft	5.19
wing area S, ft^2	36.144
x_{rp}, in	66.240
y_{rp}, in	0.000
z_{rp}, in	0.000
x_{cg}, in	69.193
y_{cg}, in	0.019
z_{cg}, in	–0.547
mass m, slugs	87.75
I_x, slugs-ft^2	54.46
I_y, slugs-ft^2	851.40
I_z, slugs-ft^2	880.37
I_{xz}, slugs-ft^2	23.51

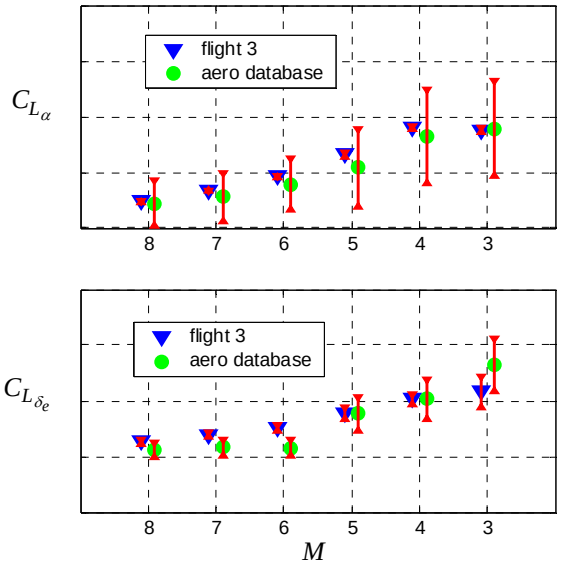

Figure 7 Lift parameters

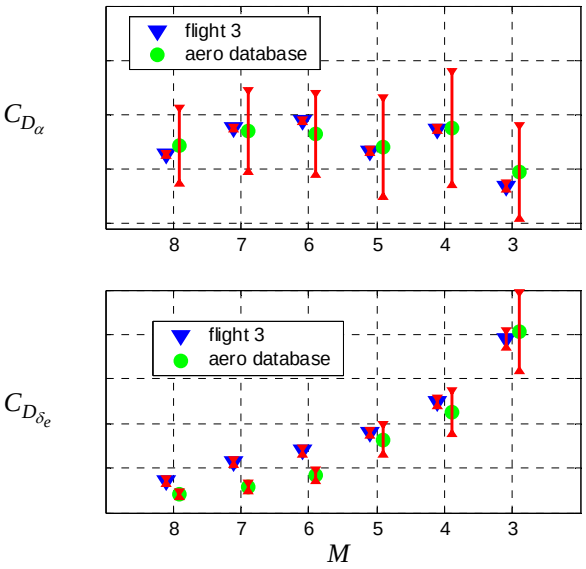

Figure 8 Drag parameters

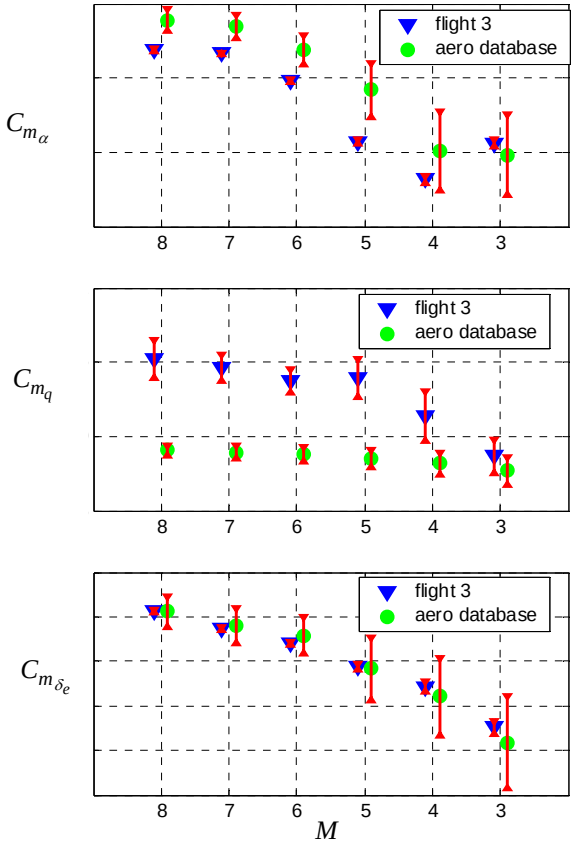

Figure 9 Pitching moment parameters

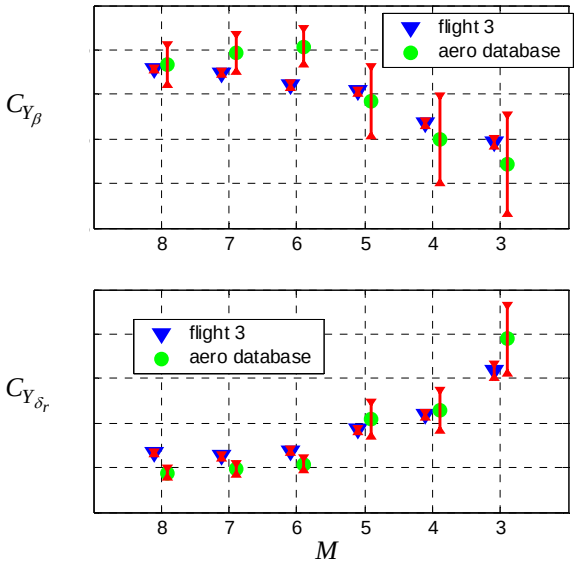

Figure 10 Side force parameters

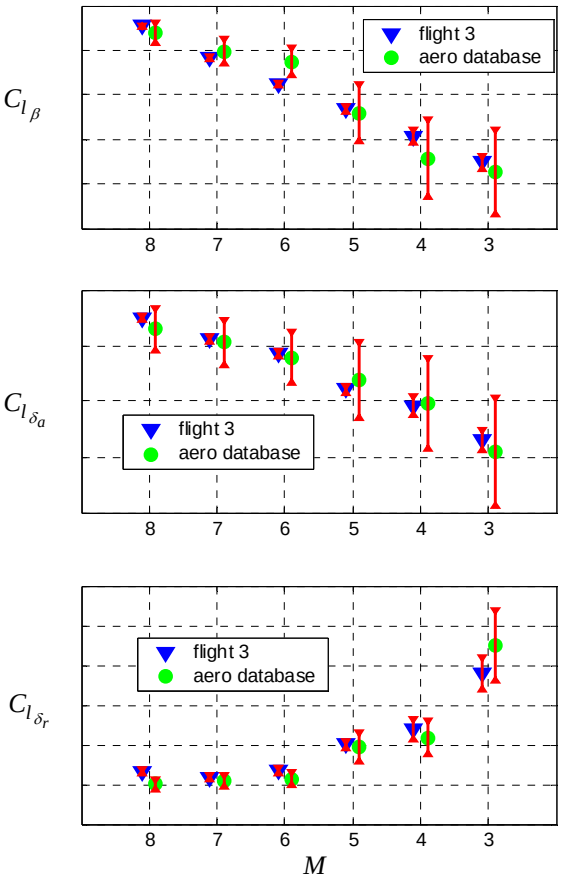

Figure 11 Rolling moment parameters

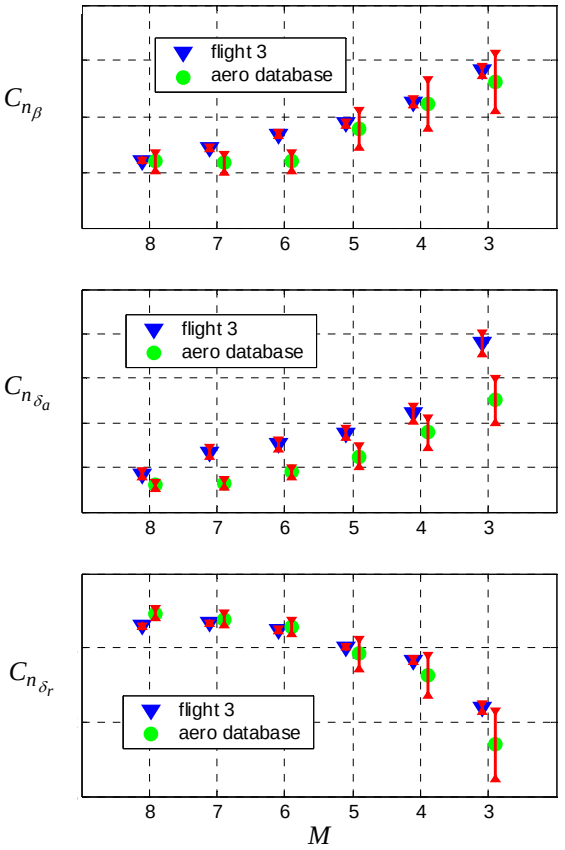

Figure 12 Yawing moment parameters

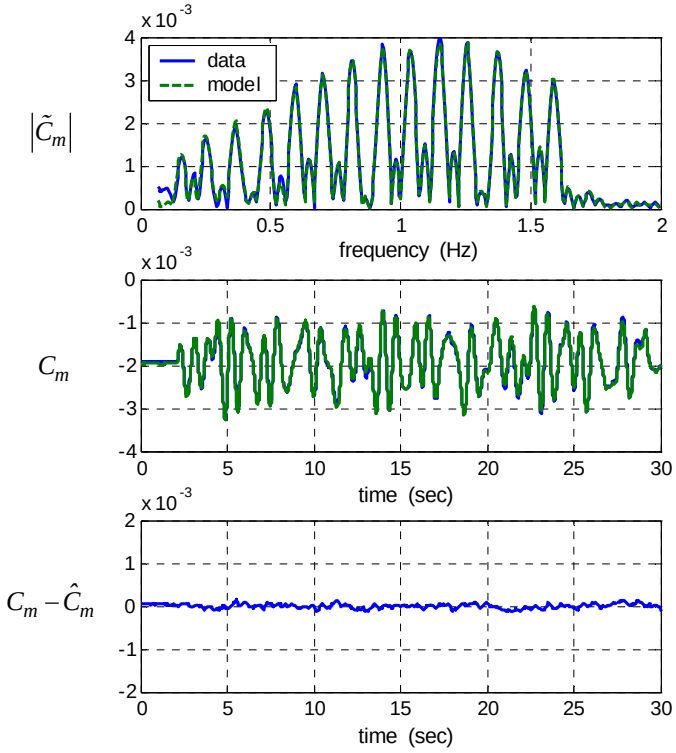

Figure 13 Model fit to pitching moment data, Mach 5

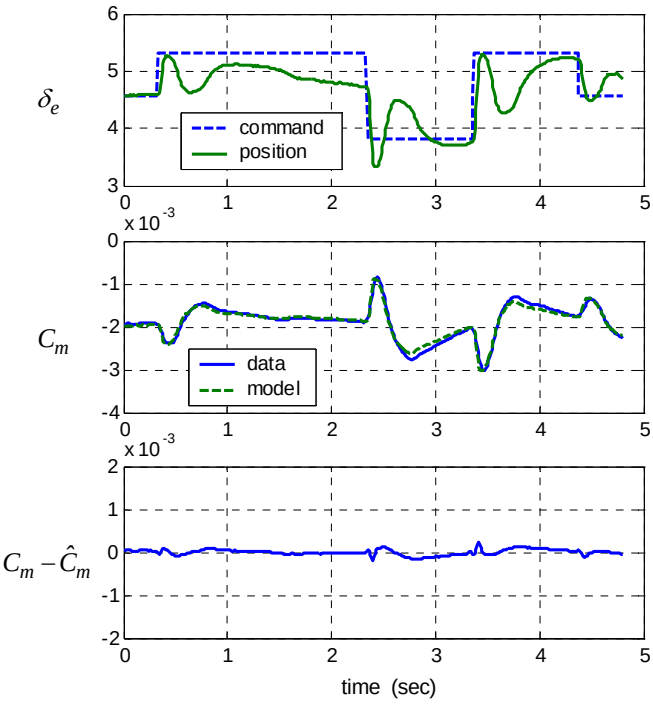

Figure 14 Model prediction of pitching moment data, Mach 5

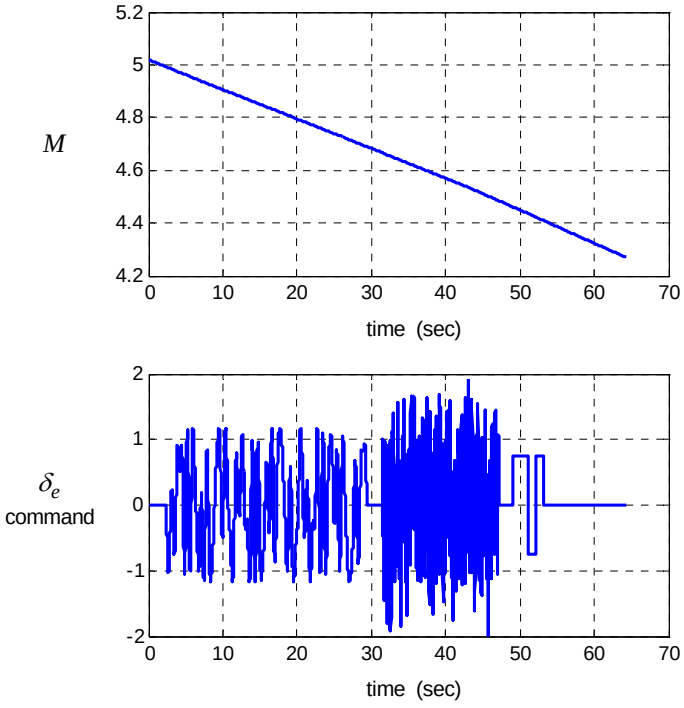

Figure 15 Mach number variation, Mach 5 maneuvers